

## Organometallic Chemistry

## Solid-State NMR and DFT Studies on the Formation of Well-Defined Silica-Supported Tantallaaziridines: From Synthesis to Catalytic Application

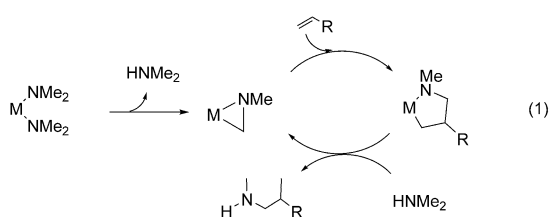
Bilel Hamzaoui, Jérémie D. A. Pelletier, Edy Abou-Hamad, Yin Chen, Mohamed El Eter, Edrisse Chermak, Luigi Cavallo, and Jean-Marie Basset\*<sup>[a]</sup>

**Abstract:** Single-site, well-defined, silica-supported tantallaaziridine intermediates  $[\equiv\text{Si-O-Ta}(\eta^2\text{-NRCH}_2)(\text{NMe}_2)_2]$  [R = Me (2), Ph (3)] were prepared from silica-supported tetrakis(dimethylamido)tantalum  $[\equiv\text{Si-O-Ta}(\text{NMe}_2)_4]$  (1) and fully characterized by FTIR spectroscopy, elemental analysis, and  $^1\text{H}$ ,  $^{13}\text{C}$  HETCOR and DQ TQ solid-state (SS) NMR spectroscopy. The

formation mechanism, by  $\beta$ -H abstraction, was investigated by SS NMR spectroscopy and supported by DFT calculations. The C–H activation of the dimethylamido ligand is favored for R = Ph. The results from catalytic testing in the hydroaminoalkylation of alkenes were consistent with the *N*-alkyl aryl amine substrates being more efficient than *N*-dialkyl amines.

## Introduction

Metallaaziridine complexes have attracted increasing attention as models for key intermediates in reactions involving metal amide species.<sup>[1]</sup> The formation mechanism of M–C bonds observed for complexes  $M(\eta^2\text{-NRCHR}')$  (R = alkyl, R' = H, alkyl) from homoleptic  $M(\text{NR}_2)_n$  is a fascinating organometallic process. It is particularly relevant to hydroaminoalkylation catalysis, in which olefins are incorporated into the metal–carbon bond of metallaaziridine complexes [Eq. (1)]. This reaction is regarded as a highly atom economical method for synthesizing a broad range of substituted secondary amines under relatively mild conditions.



Complexes of Groups 4,<sup>[2]</sup> 5,<sup>[2d,3]</sup> and 8<sup>[4]</sup> have been documented as efficient catalysts for hydroaminoalkylation. A general mechanism was initially proposed by Nugent et al. on the basis of deuterium exchange experiments with homoleptic

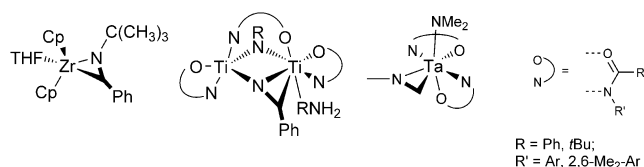
early transition metal dialkylamido complexes  $[M(\text{NR}_2)_4]$  (M = Zr, Nb, etc.; R = Me, Et).<sup>[2b]</sup> Deuterium incorporation at the  $\alpha$  position to the nitrogen atom was consistently observed and proved the formation (by  $\beta$ -H elimination) of a transient metallaaziridine complex intermediate. Since then, metallaaziridine complexes of various transition metals have been involved in several organic transformations. Examples of such stoichiometric reactions have been reported by Buchwald et al.,<sup>[5]</sup> Norton et al.,<sup>[6]</sup> Whitby et al.,<sup>[7]</sup> and Blagg et al.<sup>[7d,8]</sup> Typically, metallaaziridines can generate, after workup, functionalized amines by reaction with unsaturated C–C bonds (olefins and acetylenes) and C–X bonds (aldehydes, carbonates, and imines).

These results fueled interest in a better understanding of the reaction mechanism, with a view to improving the reactivity and selectivity of the catalysts. A series of mechanistic investigations have been reported including kinetic studies,<sup>[9]</sup> isotope distribution studies,<sup>[2b]</sup> and solid-state (SS) NMR experiments.<sup>[16]</sup> The formation of metallaaziridine intermediates was postulated as the key step in the catalytic cycle. Such species have been formally elucidated in only a few reports.<sup>[10]</sup> For instance,  $[\text{Cp}^*\text{Ta}(\text{NMe}_2)\text{Me}_3]$  undergoes intramolecular  $\beta$ -H migration to give  $[\text{Cp}^*\text{Ta}(\eta^2\text{-CH}_2\text{NMe}_2)\text{Me}_2]$  with release of methane.<sup>[11]</sup> Similar azametallacyclopropane complexes have been isolated and structurally elucidated by single-crystal X-ray crystallography (Scheme 1).

Herzon and Hartwig examined the reactivity of tantalum amido derivatives as catalysts for the  $\alpha$ -alkylation of alkyl aryl amines and dialkyl amines with terminal olefin substrates.<sup>[3a]</sup> They showed that the selectivity of hydroaminoalkylation reactions with alkenes can be affected by the electronic properties of the amine. *N*-Aryl substrates consistently led to higher yields than the dialkyl analogues.<sup>[3a]</sup> Whitby and co-workers explained this improved reactivity by the lone pair of nitrogen being less available in *N*-aryl than in *N*-alkyl amines for donation to the

[a] B. Hamzaoui, Dr. J. D. A. Pelletier, Dr. E. Abou-Hamad, Dr. Y. Chen, Dr. M. El Eter, Dr. E. Chermak, Prof. L. Cavallo, Prof. J.-M. Basset King Abdullah University of Science and Technology (KAUST) KAUST Catalysis Center (KCC), Thuwal, 23955-6900, (Saudi Arabia) E-mail: jeanmarie.basset@kaust.edu.sa

Supporting information for this article is available on the WWW under <http://dx.doi.org/10.1002/chem.201504439>.



**Scheme 1.** Previously reported molecular metallaaziridine complexes of Group 4 and 5 transition metals.

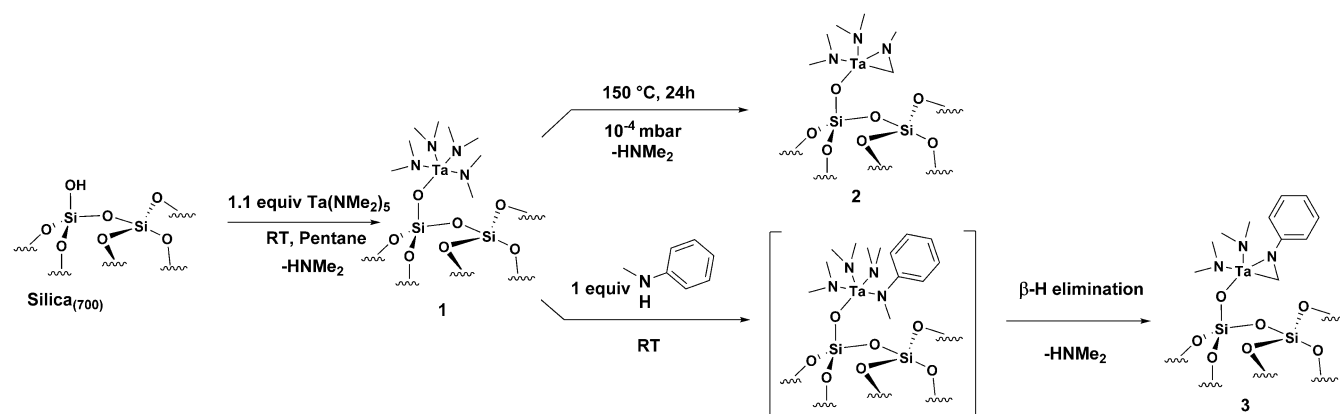
metal center due to conjugation with the aromatic  $\pi$  system.<sup>[7a]</sup> This observation is in agreement with the work by Herzon and Hartwig in which  $[\text{Ta}(\text{NMe}_2)_5]$  and  $[\{\text{Cl}_3\text{Ta}(\text{NMePh})_2\}_2]$  were tested as precatalysts for the reaction of *N*-(methyl- $d_3$ )-aniline with 1-octene. Interestingly, the highest degree of incorporation of deuterium on the  $\alpha$ -carbon atom was observed when  $[\{\text{Cl}_3\text{Ta}(\text{NMePh})_2\}_2]$  was used as precatalyst.<sup>[12]</sup> Molecular metallaaziridine complexes have been documented for two decades, but have only recently been explored within the framework of surface organometallic chemistry. This field has a solid track record in isolating and identifying transition metal catalysts with unusual reactivities.<sup>[13]</sup> Recent advances include the isolation of single-site, well-defined surface species such as  $[\equiv\text{Si}-\text{O}-\text{Ta}(=\text{CH}_2)\text{Me}_2]$  (an active catalyst for alkane metathesis)<sup>[14]</sup> and  $[\equiv\text{Si}-\text{O}-\text{Zr}(\text{HNMe}_2)(\eta^2\text{NMeCH}_2)(\text{NMe}_2)]$ .<sup>[15]</sup> The reactivity of the latter species was harnessed, and the surface monohydride  $[\equiv\text{Si}-\text{O}-\text{Zr}(\text{HNMe}_2)(\text{NMe}_2)_2\text{H}]$  was selectively isolated and shown to be an active catalyst for alkene hydrogenation.<sup>[15a]</sup> Additional studies revealed that  $[\equiv\text{Si}-\text{O}-\text{Zr}(\text{HNMe}_2)(\eta^2\text{-NMeCH}_2)(\text{NMe}_2)]$  was able to catalyze the hydroaminoalkylation of propylene with dimethylamide, albeit in modest yields.<sup>[16]</sup>

These results encouraged us to study surface metallaaziridine complexes as other candidates for surface hydroaminoalkylation catalysts. Tantalum was considered first due to the better performance of its molecular complexes over zirconium counterparts.<sup>[2b,3a]</sup> The effect of the substrate employed (*N*-di-alkyl versus *N*-alkyl *N*-aryl) over the performance of active catalytic species was also of interest (see above). Herein, we report the preparation and the characterization of the first single-site, well-defined, silica-supported tantalumaziridines  $[\equiv\text{Si}-\text{O}-$

$\text{Ta}(\eta^2\text{-NRCH}_2)(\text{NMe}_2)_2]$  [ $\text{R}=\text{Me}$  (**2**),  $\text{Ph}$  (**3**)] (Scheme 2) starting from  $[\equiv\text{Si}-\text{O}-\text{Ta}(\text{NMe}_2)_4]$  (**1**). All surface species were characterized by SS NMR spectroscopy, elemental analysis, and FTIR spectroscopy.

## Results and Discussion

Treating  $\text{SiO}_{2-(700)}$  with pentakis(dimethylamido)tantalum in pentane at ambient temperature for 1 h led to the formation of **1** as a yellow powder. Comparison of FTIR spectra of  $\text{SiO}_{2-(700)}$  and **1** indicated grafting of  $[\text{Ta}(\text{NMe}_2)_5]$  onto silica. The signal corresponding to the isolated silanol groups in  $\text{SiO}_{2-(700)}$  ( $3745\text{ cm}^{-1}\nu_{\text{O-H}}$ ) completely disappeared in **1**. New bands appeared in the regions corresponding to  $\nu_{\text{(C-H)}}$  ( $3000\text{--}2800\text{ cm}^{-1}$ ) and  $\delta_{\text{C-H}}$  ( $1500\text{--}1300\text{ cm}^{-1}$ ). They can be assigned to dimethylamine ligand vibrations (Figure 1).<sup>[15b]</sup> The combination and overtone bands of the silica ( $1990$ ,  $1867$ , and  $1639\text{ cm}^{-1}$ ) remained unchanged (Figure 1). Elemental analysis of **1** gave 4.8% Ta, 2.7% C, and 1.6% N with a molar ratio of  $\text{Ta}/\text{C}/\text{N}=1/8.4/4.2 (\pm 0.3)$ . Considering the amounts of grafted tantalum and silanol groups available for grafting (0.27 and 0.30 mmol, respectively) and the disappearance of vibrations due to silanol groups, we can propose that for **1** a tantalum complex was grafted to most of the isolated silanol groups. The Ta/N ratio of  $1/4.2 (\pm 0.3)$  is consistent with a monopodal surface complex with four  $\text{NMe}_2$  ligands. The  $^1\text{H}$  SS NMR spectrum of **1** exhibits a single broad signal centered at 3.2 ppm (Supporting Information, Figure S1);  $^{13}\text{C}$  SS NMR spectroscopy revealed one major signal at 45 ppm (Supporting Information, Figure S2). Both spectra are consistent with quasi-equivalent  $\text{CH}_3$  fragments bound to nitrogen atoms.<sup>[11]</sup> A tetrakis-dimethylamido monopodal structure  $[\equiv\text{Si}-\text{O}-\text{Ta}(\text{NMe}_2)_4]$  can be confirmed for tantalum surface complex **1** (formally  $d^0$  10e). Interestingly, a small peak at 35 ppm ( $^{13}\text{C}$  SS NMR) and a shoulder at 2.5 ppm ( $^1\text{H}$  SS NMR) can be interpreted as one  $\text{NMe}_2$  group in axial position.<sup>[11]</sup> This result illustrates a slightly different reactivity than that observed in our previous studies on the grafting of  $[\text{Zr}(\text{NMe}_2)_4]$  on  $\text{SBA}_{15-(700)}$  (formally  $d^0$  8e).<sup>[15b]</sup> In this case, the azametallacyclopropane fragment is formed spontaneously at room temperature to afford  $[\equiv\text{Si}-\text{O}-\text{Zr}(\eta^2-$



**Scheme 2.** Preparation pathways of **1–3**.  $\text{SiO}_{2-(700)}$ : silica partially dehydroxylated at  $700^\circ\text{C}$ .

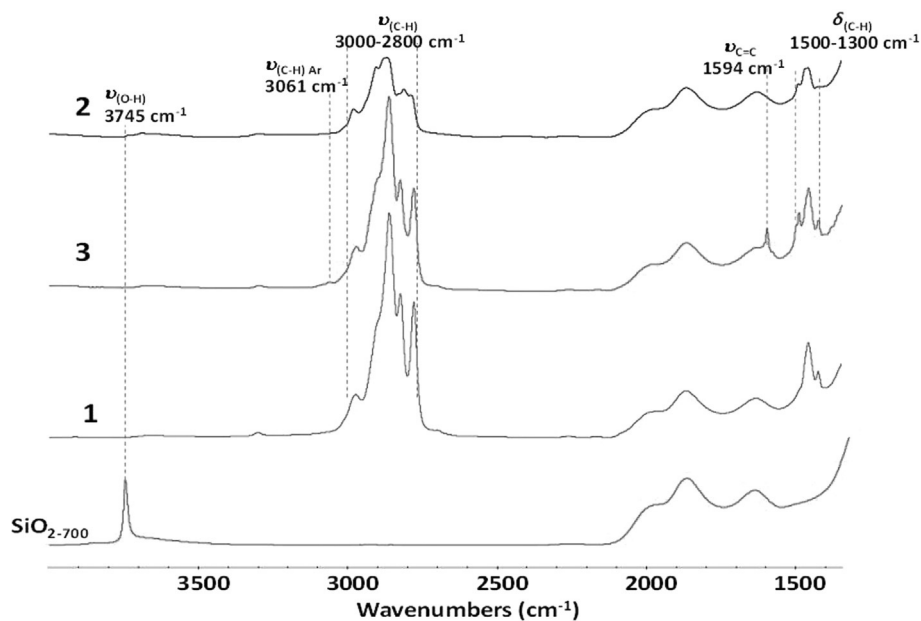


Figure 1. FTIR spectra of  $\text{SiO}_{2-700}$  and 1–3.

$\text{NMeCH}_2(\text{NHMe}_2)\text{NMe}_2]$  (formally  $d^0$  10e, like **1**). Both zirconium and tantalum dimethylamido complexes exhibit similar tendencies towards  $\beta$ -hydride elimination and metallocyclization. The lower reactivity of zirconium complexes is explained by coordination of one  $\text{HNMe}_2$  ligand released during grafting. It was rationalized that the lower reactivity of  $[\equiv\text{Si-O-Ta}(\text{NMe}_2)_4]$  regarding activation of the *N*-methyl ligand might be overcome by controlled heating under vacuum. Thermal treatment of **1** was conducted at  $10^{-4}$  mbar (Scheme 2) to give **2**. Initial evacuation of **1** at room temperature left the IR spectrum unchanged, although evacuation at a higher temperature ( $150^\circ\text{C}$ ) resulted in diminishing intensity of signals in the alkyl vibration region (Figure 1). The volatile substances identified by GC consisted exclusively of  $\text{HNMe}_2$ . Elemental analysis of **2** gave 4.8% Ta, 2.0% C, and 1.2% N with a Ta/C/N ratio of 1/6.1/3.1 ( $\pm 0.3$ ). This strongly suggests that one molecule of  $\text{HNMe}_2$  was eliminated from **1**.

Furthermore, a new band was observed at  $1490\text{ cm}^{-1}$  and the small band of **1** visible at  $1422\text{ cm}^{-1}$  disappeared in **2**. These bands correspond to vibration of the C–H bond of the  $\text{CH}_2$  group formed in **2**.<sup>[16]</sup> In comparison to  $[\equiv\text{Si-O-Zr}(\text{HNMe}_2)(\eta^2\text{-NMeCH}_2)(\text{NMe}_2)_2]$ , the wavenumber of this  $\text{CH}_2$  band is lower, as expected.

Both  $^1\text{H}$  and  $^{13}\text{C}$  SS NMR spectra of **2** are notably more complex than that of **1**. The  $^1\text{H}$  NMR spectrum of **2** contains an intense peak at 2.3 ppm and a broad peak at 3.2 ppm (Figure 2A). The 2.3 ppm signal is attributed to the  $\text{NCH}_3$  fragments, as in **1**. The resonance at 3.2 ppm can be assigned tentatively to the  $\text{TaCH}_2$  moieties (the  $\text{ZrCH}_2$  analogue shows a similar resonance at 3.2 ppm).<sup>[15b]</sup> The  $^{13}\text{C}$  SS NMR spectra of the solid product shows two signals: a large one at 34 ppm and a smaller one at 45 ppm (Figure 2B). These two peaks are reminiscent of those previously seen for zirconium,<sup>[15b]</sup> except for the absence of the broad signal corresponding to the  $\text{CH}_2$

group at 85 ppm. It is known that the signals of such methylene groups with highly restricted mobility are difficult to detect by SS NMR.<sup>[17]</sup> The HETCOR spectrum revealed a clear correlation between the proton signal at 2.3 ppm and the carbon signals at 34 and 45 ppm (Figure 2E), which confirms that all the signals observed in the  $^{13}\text{C}$  SS NMR spectrum can be assigned to NMe carbon atoms. The  $^1\text{H},^1\text{H}$  double-quantum (DQ) and triple-quantum (TQ) methods were applied to **2** to confirm the presence of the  $\text{TaCH}_2$  fragment (Figure 2C and 2D). The peak at 3.2 ppm shows autocorrelation in the DQ spectrum but not in the TQ spectrum, and it can be thus assigned to a  $\text{TaCH}_2$  fragment. Examples of NMR characterization of related molecular complexes containing an  $\text{MCH}_2$  fragment have been documented;<sup>[18]</sup> the corresponding  $^1\text{H}$  signal has been observed in the range of 1.08–2.07 ppm, slightly lower than that observed for **2**.

The peak at 2.3 ppm displays a strong autocorrelation, validating the  $\text{NMe}_2$  assignment. Thus, we can propose with certainty the structure  $[\equiv\text{Si-O-Ta}(\eta^2\text{-NMeCH}_2)(\text{NMe}_2)_2]$  for **2**. Its formation can be explained by an intramolecular  $\beta$ -H abstraction of one dimethylamido ligand (Scheme 2). This pathway has strong similarities to that described for  $[\equiv\text{Si-O-Zr}(\text{HNMe}_2)(\eta^2\text{-NMeCH}_2)(\text{NMe}_2)_2]$ , but requires more intense conditions ( $150^\circ\text{C}$  versus RT). Taking in account the work of Whitby et al.,<sup>[7a]</sup> we postulated that substituting an  $\text{NMe}(\text{alkyl})$  ligand by an  $\text{NMePh}$  ligand may improve the reactivity of the corresponding grafted species toward the formation of the tantalaaaziridine complex. Hence,  $[\equiv\text{Si-O-Ta}(\text{NMe}_2)_4]$  (**1**) was treated with one equivalent of methyl(phenyl)amine in pentane at room temperature. After 4 h of reaction, the powder was washed three times with pentane and the volatile substances were removed in vacuo. The resulting powder had a brighter yellow color than **1**. The exclusive gas-phase product detected by GC was  $\text{HNMe}_2$ . FTIR spectra of the solid prod-

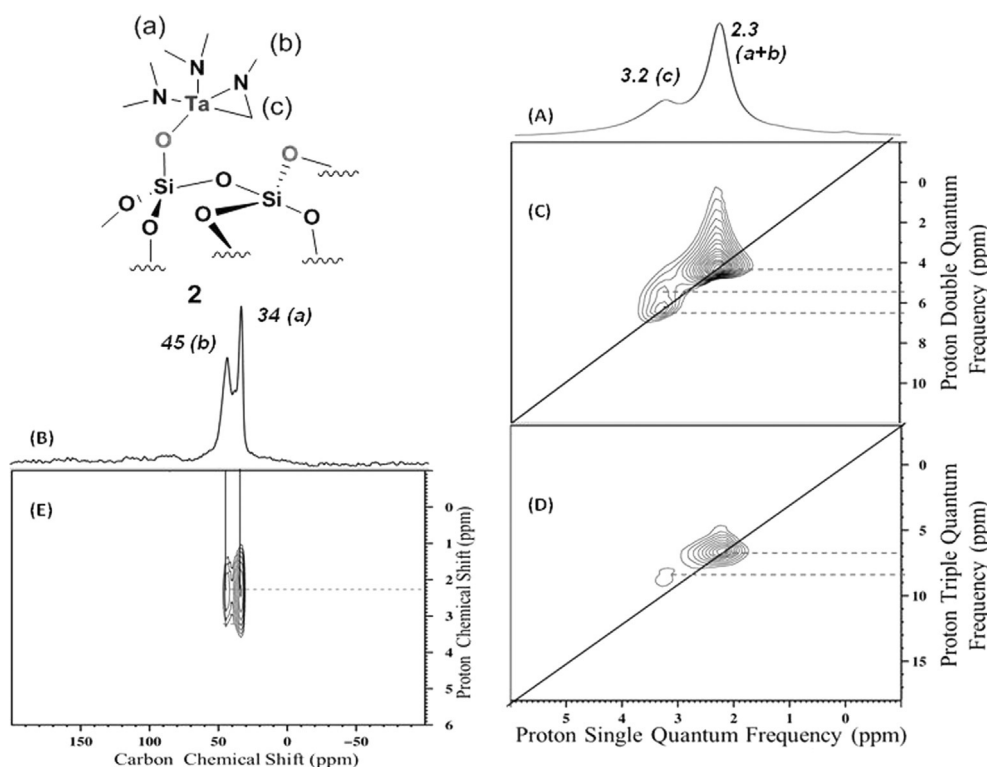


**Figure 2.** A) 1D  $^1\text{H}$  spin-echo MAS SS NMR spectrum of **2**. B)  $^{13}\text{C}$  CP/MAS NMR spectrum of **2**. C) 2D  $^1\text{H}$ ,  $^1\text{H}$  DQ/SQ, D)  $^1\text{H}$ ,  $^1\text{H}$  TQ/SQ, and E) 2D CP/MAS HETCOR NMR spectra (see Supporting Information for details).

uct **3** showed that the bands characteristic of the aryl amide ligands are clearly visible (Figure 1). A very broad signal at  $3061\text{ cm}^{-1}$  (aromatic CH bending) and another sharp one at  $1594\text{ cm}^{-1}$  ( $\nu_{\text{C}=\text{C}}$ ) could be detected. Elemental analysis of **3** gave 5.1% Ta, 3.8% C, and 1.3% N with a Ta/C/N ratio of 1/11.2/3.2 ( $\pm 0.3$ ). This indicates that methyl(phenyl)amine reacted with **1**. The  $^1\text{H}$  SS NMR spectrum of **3** (Figure 3A) exhibits predominantly one major signal at 3.4 ppm with two overlapping minor ones at 2.0 and 6.9 ppm. The  $^{13}\text{C}$  SS NMR spectrum (Figure 3B) shows one very intense resonance at 45 ppm overlapping with a weaker one at 35 ppm in addition to two small signals at 117 and 128 ppm. The two last-named resonances have chemical shifts consistent with overlapping aromatic carbon resonances, compatible with the resonance at 6.9 ppm in the  $^1\text{H}$  NMR (Figure 3A).

This is confirmed by the correlation observed in the HETCOR spectrum between these  $^1\text{H}$  and  $^{13}\text{C}$  signals (Figure 3E). Moreover, the DQ and TQ experiments showed no autocorrelation for the 6.9 ppm resonance, as expected for a CH proton (Figure 3C and 3D). These observations are in line with the presence of an aromatic ligand in **3**. The HETCOR spectrum indicates a correlation between the signals at 35 and 45 ppm ( $^{13}\text{C}$  SS NMR) and that at 3.4 ppm in the  $^1\text{H}$  SS NMR spectrum (Figure 3E). Furthermore, the DQ and TQ spectra both show autocorrelation for the 3.4 ppm resonance, confirming the presence of  $\text{CH}_3$  fragments (Figure 3C and D). Hence, the signals can be assigned to  $\text{NCH}_3$  of the aminomethyl ligands. Finally, the signal at 2.0 ppm ( $^1\text{H}$ ) autocorrelates in the DQ but not in the TQ spectrum and can thus be attributed to a  $\text{CH}_2$  group.<sup>[19]</sup> Its

chemical shift is smaller than that of **2** (3.2 ppm). This can be explained by the presence of the aromatic ring in **3**. Indeed, the mesomeric effects of the aromatic ring (as an electron donor) can induce a shift to lower frequency.<sup>[7a]</sup> Note that generation of an  $\eta^2$ -imine complex by activation of the methyl group of the amido ligand occurred at room temperature in this case.

To shed light on the generation mechanism of the metallaaziridines  $[\equiv\text{Si}-\text{O}-\text{Ta}(\eta^2\text{-NMeCH}_2)(\text{NMe}_2)_2]$  (**2**) and  $[\equiv\text{Si}-\text{O}-\text{Ta}(\eta^2\text{NPhCH}_2)(\text{NMe}_2)_2]$  (**3**) from  $[\equiv\text{Si}-\text{O}-\text{Ta}(\text{NMe}_2)_4]$  (**1**), DFT calculations were conducted for their respective formation pathways including  $\beta$ -hydride elimination. Consistent with previous work validating the cluster model,<sup>[20]</sup> the surface of the silica support was modeled by a silsesquioxane  $\text{Si}_8\text{O}_{12}\text{H}_8$  cage structure with one  $[\equiv\text{Si}-\text{O}-\text{Ta}(\text{NMe}_2)_4]$  moiety grafted to one of the SiOH groups (see Figure 4). The initial  $[\equiv\text{Si}-\text{O}-\text{Ta}(\text{NMe}_2)_4]$  species (**1**) was considered as the reference structure at  $0\text{ kcal mol}^{-1}$ . The formation of metallacyclic species **2** and **3** was found to follow two different reaction pathways (Figure 5). For that leading to methyl-substituted metallaaziridine **2** (blue in Figure 5), a transition state (**1-2** in Figure 5) was considered corresponding to the transfer of a hydrogen atom from the carbon atom of one of the  $\text{NMe}_2$  ligands to the nitrogen atom of another  $\text{NMe}_2$  ligand.

The overall geometry of the ligands around the tantalum center in **1-2** is best described as octahedral. Transition state **1-2** is located  $32.8\text{ kcal mol}^{-1}$  above the starting species **1**. This relatively high barrier is in agreement with the experimental reaction requiring heating at  $150^\circ\text{C}$ . Converging the geometry

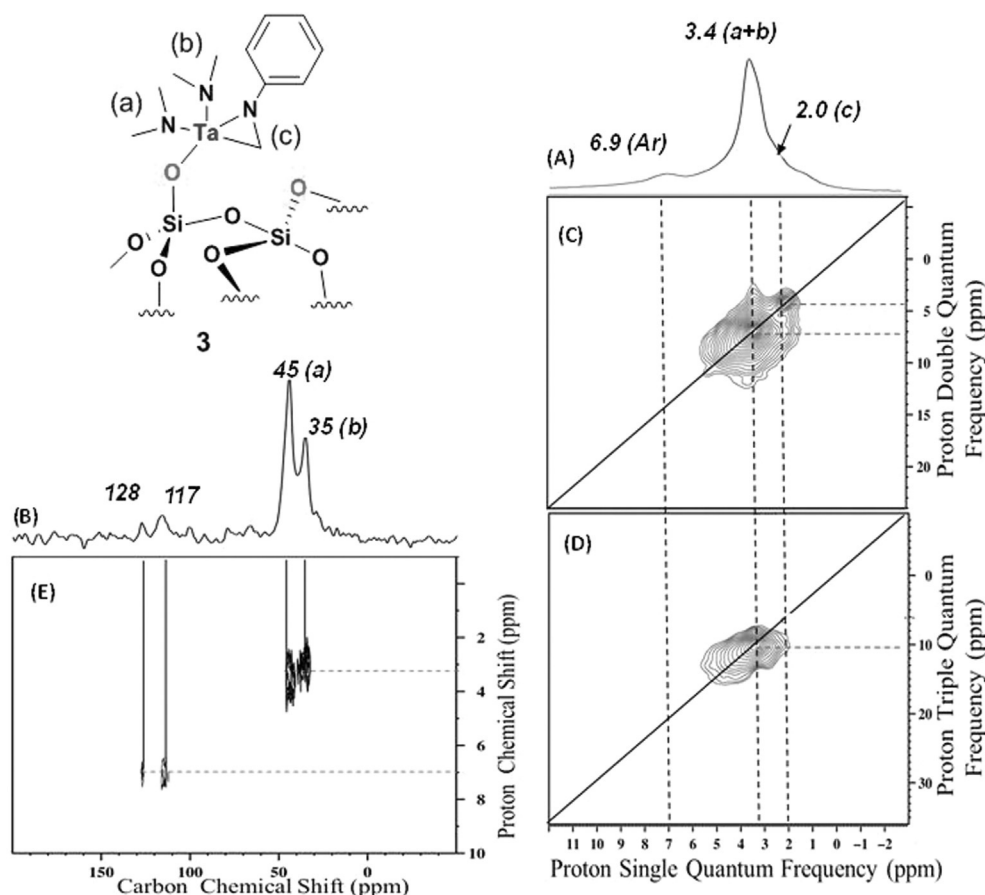


**Figure 3.** A) 1D  $^1\text{H}$  spin-echo MAS SS NMR spectrum of **3**. B)  $^{13}\text{C}$  CP/MAS NMR spectrum of **3**. C) 2D  $^1\text{H},^1\text{H}$  DQ/SQ, D)  $^1\text{H},^1\text{H}$  TQ/SQ, and E) 2D CP/MAS HETCOR NMR spectrum (see Supporting Information for details).

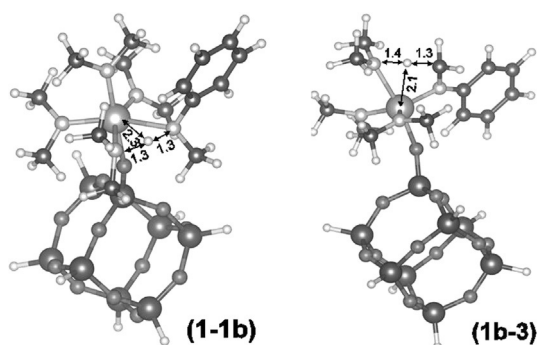


**Figure 4.** Structures of key transition states along the reaction pathway involving HN(Ph)(Me) with some distances [Å].

of transition state **1-2** onto the products side leads then to the dissociation of  $\text{HNMe}_2$  and the formation of metallacycle **2**; the total Gibbs free-energy cost is  $18.0 \text{ kcal mol}^{-1}$  relative to the initial species **1**.

For the pathway leading to phenyl-substituted metallazaaziridine (green in Figure 5), two steps were considered starting with the ligand exchange between  $\text{NMe}_2$  and  $\text{NPhMe}$  followed by the  $\beta\text{-H}$  elimination.  $\text{HN(Ph)(Me)}$  can replace a  $\text{NMe}_2$  ligand on the tantalum center of **1** leading to intermediate  $[\equiv\text{Si-O-$

$\text{Ta(NMe}_2)_3(\text{NPhMe})]$  (**1b**), which has not been observed experimentally. The second step consists of hydrogen transfer from the  $\text{NPhMe}$  ligand to one of the  $\text{NMe}_2$  ligands, similar to the conversion of **1** to **2**. In the first step, transition state **1-1b** has an energy barrier of  $21.2 \text{ kcal mol}^{-1}$  relative to the initial structure **1**. This relatively low barrier is consistent with the reaction occurring at room temperature. Transition state **1-1b** involves hydrogen transfer from the nitrogen atom of the external  $\text{HN(Ph)(Me)}$  ligand to the nitrogen atom of one of the  $\text{NMe}_2$  ligands. This hydrogen transfer leads to the dissociation of  $\text{HNMe}_2$  and to the formation of intermediate **1b**, which lies above **1** by  $2.9 \text{ kcal mol}^{-1}$ . The second transition state **1b-3** (Figure 5) is obtained by hydrogen transfer between the carbon atom of the  $\text{N(Ph)(Me)}$  ligand to one of the  $\text{NMe}_2$  ligands, leading to metallacycle **3**. Transition state **1b-3** is located  $30.1$  and  $27.2 \text{ kcal mol}^{-1}$  above **1** and **1b**, respectively. It is noteworthy that the reaction was run under high vacuum, in which the formed  $\text{HNMe}_2$  is removed. Hence, it can be assumed that the most correct estimate for the overall barrier corresponding to the formation of **3** is that of  $27.2 \text{ kcal mol}^{-1}$  corresponding to the energy difference between transition state **1b-3** and intermediate **1b**, rather than the largest energy difference between the highest-energy transition state **1b-3** and the most stable intermediate **1** ( $30.1 \text{ kcal mol}^{-1}$ ). In this scenario, the barrier of  $27.2 \text{ kcal mol}^{-1}$  can nonetheless be

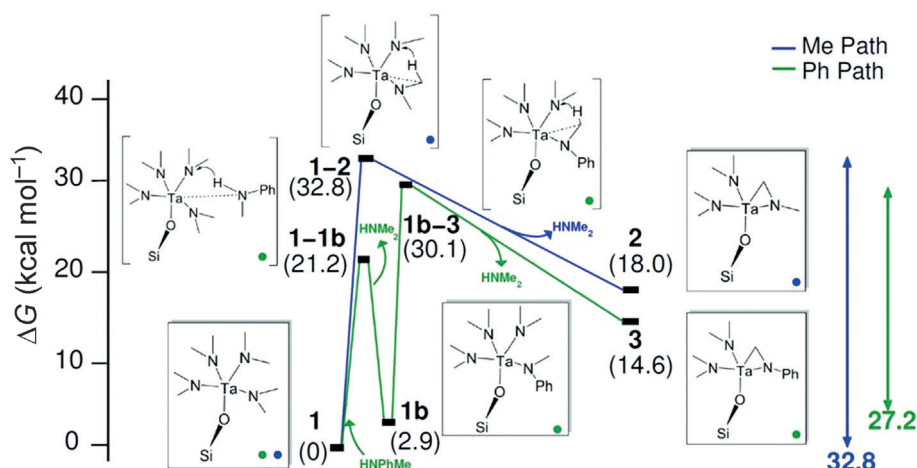


Figure 5. DFT reaction profiles for the transformation of **1** into **2** or **3**.

considered consistent with this reaction occurring at room temperature. Finally, converging transition state **1b-3** on the products side leads to the  $[\equiv\text{Si}-\text{O}-\text{Ta}(\eta^2\text{-NPhCH}_2)(\text{NMe}_2)_2]$  metallacycle **3**,  $14.6 \text{ kcal mol}^{-1}$  above **1** in terms of free energy. In conclusion, our calculations show that the presence of an aryl group on the  $\text{NR}_2$  ligand reduces the free-energy barrier for metallacycle formation from  $32.8$  to  $27.2 \text{ kcal mol}^{-1}$ , which follows the trend of the experimental observations.

Further, we also carried out DFT-based NMR calculations to strengthen the assignments of the NMR peaks (Supporting Information, Table S5). Corroborating the interpretation of the experimental results, the calculated chemical shifts of the C atom of the metallacycle  $\text{TaCH}_2$  moiety in **2** and **3** (respectively  $61.0$  and  $58.2 \text{ ppm}$ ) are shifted by roughly  $10 \text{ ppm}$  relative to the average chemical shift of the C atoms of the Me groups of  $\text{TaNMe}_2$  in **2** and **3** ( $47.80$  and  $48.08 \text{ ppm}$ , respectively).

Species **1-3** were considered as catalysts for hydroamination reactions. The screening was conducted with selected substrates such as dialkyl amines ( $\text{HNMeR}$ ;  $\text{R}=\text{Pr}$ ,  $i\text{Bu}$ ) and  $N$ -methyl anilines ( $\text{HNMe}(4\text{-R-Ar})$ ;  $\text{R}=\text{H}$ ,  $\text{OMe}$ ,  $\text{OCF}_3$ ,  $\text{Cl}$ ). All runs were carried out under similar conditions [ $165^\circ\text{C}$ , 1-octene (1.5 equiv), 4 mol% catalyst, toluene (0.4 mL)] and terminated after 1, 3, or 6 d (Table 1). Since the branched alkylation products were the sole regioisomers detected, insertion occurring in 1,2 fashion. Precatalysts **1-3** were screened with methyl-(phenyl)amine and formed the branched hydroaminoalkylation product (Table 1, entries 1–3). All precatalysts resulted in comparable yields (typically about 45% after 6 d) regardless of the duration of the experiments. This indicates that the catalytically active species is likely to be the same in Table 1 (entries 1–3) and assumed to be **3**.

Reactions with electron-rich  $N$ -methylanilines such as (4-chlorophenyl)methylamine (Table 1, entry 4), (4-methoxyphenyl)methylamine (Table 1, entry 5), and methyl[4-(trifluoromethoxy)phenyl]amine (Table 1, entry 6), occurred in slightly higher yields (around 50% after 6 d). The introduction of an electron-withdrawing substituent on the *para* position of the  $N$ -aryl ligand seems to have a limited effect. Dialkyl amides such as  $N$ ,2-dimethyl-1-propanamine (Table 1, entry 7) and

Table 1. Hydroamination substrate testing with catalysts **1-3**.

$\text{R}_1\text{N}(\text{CH}_3)\text{H} + \text{CH}_2=\text{CH}-n\text{-hexyl} \xrightarrow{\text{cat. (4 mol\%)}} \text{R}_1\text{N}(\text{CH}_3)\text{H}-\text{CH}_2-\text{CH}-n\text{-hexyl}$					
Entry	Aryl amine	Catalyst	Yield <sup>[a]</sup> [%]		
			24 h	3 d	6 d
1		1	23	38	41
2		2	19	29	42
3		3	22	35	46
4		1	20	42	51
5		1	21	39	48
6		1	31	42	53
7		1	10	26	30
8		1	12	27	33
9		3	12	25	31

[a] Determined by GC-FID with amine as default product. The yields based on the olefin substrate were similar.

methyl(propyl)amine (Table 1, entry 8) reacted in lower yields (around 30% after 6 d). Thus, substituting the amine with electron-donating groups reduces the yield significantly. These results are in agreement with catalytic  $\alpha$ -alkylation of amines being more efficient with  $N$ -aryl alkyl amines than with dialkyl amines (see above).

When **3** was employed as a catalyst for the reaction involving methyl(propyl)amine (Table 1, entry 9), we detected by GC/

MS a small amount of hydroaminoalkylated product containing an aromatic group (see Supporting Information, Figure S4). We also noted the disappearance of the aromatic signals in the FTIR spectrum of the catalyst after the reaction (see Supporting Information, Figure S6). Since all hydroaminoalkylated products contain N–H bonds, the possibility that the product is adsorbed on the surface was checked by recording the FTIR spectra of the catalysts after the reaction, and no new peak in the region of the NH vibration was observed (see Supporting Information, Figure S5).

## Conclusion

Single-site, well-defined, silica-supported tetrakis(dimethylamido)tantalum [ $\equiv\text{Si-O-Ta}(\text{NMe}_2)_4$ ] (**1**) can undergo  $\beta$ -H elimination of dimethylamine leading to the corresponding silica-supported tantalazaaziridine. By combining SS NMR spectroscopy of the isolated intermediates and DFT studies on the reaction mechanism, we can conclude that the electronic properties of the amine direct the reactivity of the tantalum center. [ $\equiv\text{Si-O-Ta}(\eta^2\text{-NMeCH}_2)(\text{NMe}_2)_2$ ] (**2**) can be conveniently obtained by thermal treatment of **1** (150 °C, 24 h). In contrast, the tantalazaaziridine species [ $\equiv\text{Si-O-Ta}(\eta^2\text{-NPhCH}_2)(\text{NMe}_2)_2$ ] (**3**) can be prepared at room temperature by treatment of **1** with a methyl aryl amine. Catalytic testing of a selection of amines with various electronic properties was carried out. The  $\alpha$ -alkylation of amines was consistently more efficient with *N*-aryl *N*-alkyl amine substrates than with their dialkyl amine counterparts.

## Experimental Section

### General

All experiments were carried out under an atmosphere of argon or nitrogen. The surface species were handled by using high-vacuum lines ( $<10^{-5}$  mbar) and glovebox techniques. Elemental analyses were performed at the Microanalysis Labor Pascher and KAUST Analytical Corelab. All chemicals including  $[\text{Ta}(\text{NMe}_2)_5]$  were purchased from Sigma-Aldrich. FTIR spectra were recorded with a Nicolet 6700 FTIR spectrometer equipped with a cell designed for in situ experiments with  $\text{CaF}_2$  windows. Typically, sixteen scans were accumulated for each spectrum (resolution of  $4\text{ cm}^{-1}$ ).

### SS NMR spectroscopy

One dimensional  $^1\text{H}$  MAS and  $^{13}\text{C}$  CP-MAS solid state NMR spectra were recorded with a Bruker AVANCE III spectrometer operating at 400 MHz for  $^1\text{H}$  with a conventional double-resonance 4 mm CPMAS probe. The samples were introduced under argon into zirconia rotors, which were then tightly closed. The spinning frequency was set to 17 kHz for  $^1\text{H}$  and 10 kHz for  $^{13}\text{C}$  spectra. NMR chemical shifts are reported with respect to TMS as external reference for  $^1\text{H}$  and  $^{13}\text{C}$ . For CP/MAS  $^{13}\text{C}$  NMR, the following sequence was used:  $90^\circ$  pulses on the proton (pulse length 2.4 s), a cross-polarization step with a contact time of typically 2 ms, and finally acquisition of the  $^{13}\text{C}$  signal under high-power proton decoupling. The delay between the scans was set to 5 s to allow complete relaxation of the  $^1\text{H}$  nuclei, and the number of scans was 3000–5000 for  $^{13}\text{C}$  and 32 for  $^1\text{H}$ . An apodization function (exponential) corre-

sponding to a line broadening of 80 Hz was applied prior to Fourier transformation.

### $^1\text{H}$ , $^1\text{H}$ MQ NMR spectroscopy

Two-dimensional DQ experiments were recorded on Bruker AVANCE III spectrometer with a conventional double-resonance 3.2 mm CP/MAS probe, according to the following general scheme: excitation of DQ coherences,  $t_1$  evolution, Z filter, and detection. The spectra were recorded in a rotor-synchronized fashion in  $t_1$ , that is, the  $t_1$  increment was set equal to one rotor period (4.545  $\mu\text{s}$ ). One cycle of the standard back-to-back (BABA) recoupling sequence was used for the excitation and reconversion period. Quadrature detection in  $w_1$  was achieved by using the States-TPPI method. A spinning frequency of 22 KHz was used. The  $90^\circ$  proton pulse length was 2.5  $\mu\text{s}$ , and a recycle delay of 5 s was used. A total of 128  $t_1$  increments with 32 scans each were recorded.

### Preparation of [ $\equiv\text{Si-O-Ta}(\text{NMe}_2)_4$ ] (**1**)

In a double Schlenk vessel, 132 mg of  $\text{Ta}(\text{NMe}_2)_5$  in slight excess (1.1 equiv) with respect to the amount of surface-accessible silanol groups (0.3 mmol per gram) was treated with 1 g of  $\text{SiO}_{2-700}$  at room temperature in pentane for 1 h. After filtration and four washing cycles, all volatile compounds were evaporated and the white solid was dried for 1 h under dynamic vacuum ( $<10^{-5}$  mbar).

### Preparation of [ $\equiv\text{Si-O-Ta}(\eta^2\text{-NMeCH}_2)(\text{NMe}_2)_2$ ] (**2**)

In a glass reactor (230 mL), 1 g of **1** was heated with a gradient from room temperature to 150 °C ( $1^\circ\text{C min}^{-1}$ ) and then at 150 °C for 24 h under dynamic vacuum ( $<10^{-5}$  mbar). The resulting powder was then cooled to 22 °C and analyzed by FTIR and SS NMR spectroscopy.

### Preparation of [ $\equiv\text{Si-O-Ta}(\eta^2\text{-NPhCH}_2)(\text{NMe}_2)_2$ ] (**3**)

In a double Schlenk vessel, 0.14 mL of methyl(phenyl)amine (1 equiv) was treated with 500 mg of **1** at room temperature in pentane for 4 hr. After filtration and four washing cycles, all gas-phase products were analyzed by GC, and the solid product was dried for 1 h under dynamic vacuum ( $<10^{-5}$  mbar).

### Alkylation of *N*-alkyl aryl amines and *N*-dialkyl amines with 1-octene

Three vacuum-sealed ampoules was charged sequentially with the catalyst (0.04 equiv), toluene (400  $\mu\text{L}$ ), secondary amine (1 equiv), a Teflon-coated stir bar, and 1-octene (1.50 equiv). The ampoules were then removed from the glovebox and connected to a high-vacuum line. The mixture was condensed by cooling with liquid nitrogen and the ampoules were evacuated ( $<10^{-5}$  mbar). After sealing, the ampoules were placed in an oil bath (165 °C). The reaction mixture was heated for 1, 3, and 6 d, and each time after reaction it was cooled to 22 °C. The product solution was filtered to remove the catalyst and the remaining liquid product was analyzed by GC-FID and GC-MS.

### Computational details

All calculations were performed with Gaussian 09.<sup>[21]</sup> For geometry optimizations, transition-state searches, and vibrational-frequencies evaluations, we used the Perdew–Burke–Erznehof (PBE)<sup>[22]</sup> function-

al along with the split valence polarization basis set of Ahlrichs for main group atoms (basis set SVP in G09),<sup>[23]</sup> while for tantalum we described the core electrons with the Stuttgart SDD<sup>[23]</sup> quasirelativistic effective core potential with the associated triple- $\zeta$  basis set for valence electrons. Minima and transition states were characterized by the appropriate number of negative eigenvalues in the Hessian. We also checked that the imaginary frequency of all the transition-state structure corresponds to a vibration along the reactive path between reactants and products. We ran the final single-point energy calculations over the PBE optimized geometries using the hybrid PBE0 functional<sup>[24]</sup> with the empirical dispersion correction of Grimme (D3)<sup>[25]</sup> along with the triple- $\zeta$  valence plus one polarization function basis set of Ahlrichs (basis set TZVP in G09).<sup>[26]</sup> We evaluated the final Gibbs free energies of all stationary point of the potential-energy surface by adding the PBE0-D3/TZVP/SDD single point energies to the thermal corrections at 298.15 K, including zero-point vibrational energy at the PBE/SVP/SDD level and entropy terms. Chemical shifts relative to TMS were evaluated on the Gaussian 09 optimized geometries by using the ADF suite of programs.<sup>[27]</sup> The PBE0 functional in connection with the all-electron triple- $\zeta$  plus one polarization function basis set TZVP was used. Scalar relativistic effects were included through the ZORA Hamiltonian.<sup>[28]</sup>

## Acknowledgements

The authors wish to thank King Abdullah University of Science and Technology for continuous support.

**Keywords:** hydroamination · metallacycles · solid-state NMR spectroscopy · supported catalysts · tantalum

- [1] J. M. P. Lauzon, L. L. Schafer, *Dalton Trans.* **2012**, 41, 11539–11550.
- [2] a) M. G. Clerici, F. Maspero, *Synthesis* **1980**, 305–306; b) W. A. Nugent, D. W. Ovenall, S. J. Holmes, *Organometallics* **1983**, 2, 161–162; c) J. Dörfler, T. Preuss, A. Schischko, M. Schmidtmann, S. Doye, *Angew. Chem. Int. Ed.* **2014**, 53, 7918–7922; *Angew. Chem.* **2014**, 126, 8052–8056; d) E. Chong, L. L. Schafer, *Org. Lett.* **2013**, 15, 6002–6005; e) J. Dörfler, S. Doye, *Angew. Chem. Int. Ed.* **2013**, 52, 1806–1809; *Angew. Chem.* **2013**, 125, 1851–1854.
- [3] a) S. B. Herzon, J. F. Hartwig, *J. Am. Chem. Soc.* **2007**, 129, 6690; b) P. W. Roesky, *Angew. Chem. Int. Ed.* **2009**, 48, 4892–4894; *Angew. Chem.* **2009**, 121, 4988–4991; c) E. Chong, J. W. Brandt, L. L. Schafer, *J. Am. Chem. Soc.* **2014**, 136, 10898–10901; d) P. Eisenberger, R. O. Ayinla, J. M. P. Lauzon, L. L. Schafer, *Angew. Chem. Int. Ed.* **2009**, 48, 8361–8365; *Angew. Chem.* **2009**, 121, 8511–8515; e) P. Garcia, Y. Y. Lau, M. R. Perry, L. L. Schafer, *Angew. Chem. Int. Ed.* **2013**, 52, 9144–9148; *Angew. Chem.* **2013**, 125, 9314–9318; f) J. Dörfler, S. Doye, *Eur. J. Org. Chem.* **2014**, 2014, 2790–2797; g) G. F. Zi, F. R. Zhang, H. B. Song, *Chem. Commun.* **2010**, 46, 6296–6298; h) A. L. Reznichenko, T. J. Emge, S. Audorsch, E. G. Klauber, K. C. Hultsch, B. Schmidt, *Organometallics* **2011**, 30, 921–924.
- [4] a) D. C. Schmitt, J. Lee, A. M. R. Dechert-Schmitt, E. Yamaguchi, M. J. Kirsche, *Chem. Commun.* **2013**, 49, 6096–6098; b) T. Y. Chen, R. Tsutsumi, T. P. Montgomery, I. Volchkov, M. J. Kirsche, *J. Am. Chem. Soc.* **2015**, 137, 1798–1801.
- [5] a) R. B. Grossman, W. M. Davis, S. L. Buchwald, *J. Am. Chem. Soc.* **1991**, 113, 2321–2322; b) S. L. Buchwald, R. B. Nielsen, *J. Am. Chem. Soc.* **1988**, 110, 3171–3175; c) S. L. Buchwald, R. B. Nielsen, J. C. Dewan, *Organometallics* **1988**, 7, 2324–2328.
- [6] a) J. X. Chen, J. A. Tunge, J. R. Norton, *J. Org. Chem.* **2002**, 67, 4366–4369; b) D. A. Gately, J. R. Norton, P. A. Goodson, *J. Am. Chem. Soc.* **1995**, 117, 986–996; c) T. V. Lubben, K. Plossl, J. R. Norton, M. M. Miller, O. P. Anderson, *Organometallics* **1992**, 11, 122–127; d) J. A. Tunge, C. J. Czerwinski, D. A. Gately, J. R. Norton, *Organometallics* **2001**, 20, 254–260; e) J. A. Tunge, D. A. Gately, J. R. Norton, *J. Am. Chem. Soc.* **1999**, 121, 4520–4521.
- [7] a) N. Coles, M. C. J. Harris, R. J. Whitby, J. Blagg, *Organometallics* **1994**, 13, 190–199; b) J. M. Davis, R. J. Whitby, A. Jaxachamiec, *Tetrahedron Lett.* **1992**, 33, 5655–5658; c) J. M. Davis, R. J. Whitby, A. Jaxachamiec, *Tetrahedron Lett.* **1994**, 35, 1445–1448; d) M. C. J. Harris, R. J. Whitby, J. Blagg, *Tetrahedron Lett.* **1995**, 36, 4287–4290.
- [8] a) N. Coles, R. J. Whitby, J. Blagg, *Synlett* **1990**, 271–272; b) N. Coles, R. J. Whitby, J. Blagg, *Synlett* **1992**, 143–145.
- [9] a) I. Prochnow, P. Zark, T. Muller, S. Doye, *Angew. Chem. Int. Ed.* **2011**, 50, 6401–6405; *Angew. Chem.* **2011**, 123, 6525–6529; b) A. L. Reznichenko, K. C. Hultsch, *J. Am. Chem. Soc.* **2012**, 134, 3300–3311.
- [10] a) L. W. Francisco, P. S. White, J. L. Templeton, *Organometallics* **1996**, 15, 5127–5136; b) L. H. Polm, G. Vankoten, C. J. Elsevier, K. Vrieze, B. F. K. Vansanten, C. H. Stam, *J. Organomet. Chem.* **1986**, 304, 353–370; c) H. Hoberg, V. Gotz, C. Kruger, Y. H. Tsay, *J. Organomet. Chem.* **1979**, 169, 209–217; d) J. Browning, H. D. Empsall, M. Green, F. G. A. Stone, *J. Chem. Soc. Dalton Trans.* **1973**, 381–387.
- [11] J. M. Mayer, C. J. Curtis, J. E. Bercaw, *J. Am. Chem. Soc.* **1983**, 105, 2651–2660.
- [12] S. B. Herzon, J. F. Hartwig, *J. Am. Chem. Soc.* **2008**, 130, 14940.
- [13] J. M. Basset, S. L. Scott, L. Choplin, A. Leconte, M. Quignard, F. Santini, C. Theolier in *Organometallic Chemistry as a Basis for Understanding Heterogeneous Catalysis*, Vol. 39: *Elementary Reaction Steps in Heterogeneous Catalysis* (Eds.: R. W. Joyner and R. A. van Santen), Springer Science + Business Media, Dordrecht, **1993**, pp. 39–49.
- [14] Y. Chen, E. Abou-hamad, A. Hamieh, B. Hamzaoui, L. Emsley, J. M. Basset, *J. Am. Chem. Soc.* **2015**, 137, 588–591.
- [15] a) B. Hamzaoui, M. El Eter, E. Abou-Hamad, Y. Chen, J. D. A. Pelletier, J. M. Basset, *Chem. Eur. J.* **2015**, 21, 4294–4299; b) M. El Eter, B. Hamzaoui, E. Abou-Hamad, J. D. A. Pelletier, J. M. Basset, *Chem. Commun.* **2013**, 49, 4616–4618.
- [16] B. Hamzaoui, J. D. A. Pelletier, M. El Eter, Y. Chen, E. Abou-Hamad, J.-M. Basset, *Adv. Synth. Catal.* **2015**, 357, 3148–3154.
- [17] M. Beaudoin, S. L. Scott, *Organometallics* **2001**, 20, 237–239.
- [18] S. L. Buchwald, B. T. Watson, M. W. Wannamaker, J. C. Dewan, *J. Am. Chem. Soc.* **1989**, 111, 4486–4494.
- [19] F. A. Pasha, L. Cavallo, J. M. Basset, *ACS Catal.* **2014**, 4, 1868–1874.
- [20] a) Y. Chen, R. Credendino, E. Callens, M. Atiqullah, M. A. Al-Harhi, L. Cavallo, J.-M. Basset, *ACS Catal.* **2013**, 3, 1360–1364; b) B. Werghi, A. Bendjeriou-Sedjerari, J. Sofack-Kreutzer, A. Jedidi, E. Abou-Hamad, L. Cavallo, J.-M. Basset, *Chem. Sci.* **2015**, 6, 5456–5465; c) V. D'Elia, H. Dong, A. J. Rossini, C. M. Widdifield, S. V. C. Vummaleti, Y. Minenkov, A. Poater, E. Abou-Hamad, J. D. A. Pelletier, L. Cavallo, L. Emsley, J.-M. Basset, *J. Am. Chem. Soc.* **2015**, 137, 7728–7739; d) A. Hamieh, Y. Chen, S. Abdel-Azeim, E. Abou-hamad, S. Goh, M. Samantaray, R. Dey, L. Cavallo, J. M. Basset, *ACS Catal.* **2015**, 5, 2164–2171; e) N. Riache, A. Dery, E. Callens, A. Poater, M. Samantaray, R. Dey, J. Hong, K. Li, L. Cavallo, J.-M. Basset, *Organometallics* **2015**, 34, 690–695.
- [21] M. J. Frisch, G. W. Trucks, H. B. Schlegel, G. E. Scuseria, M. A. Robb, J. R. Cheeseman, G. Scalmani, V. Barone, B. Mennucci, G. A. Petersson, H. Nakatsuji, M. Caricato, X. Li, H. P. Hratchian, A. F. Izmaylov, J. Bloino, G. Zheng, J. L. Sonnenberg, M. Hada, M. Ehara, K. Toyota, R. Fukuda, J. Hasegawa, M. Ishida, T. Nakajima, Y. Honda, O. Kitao, H. Nakai, T. Vreven, J. A. Montgomery Jr., J. E. Peralta, F. Ogliaro, M. J. Bearpark, J. Heyd, E. N. Brothers, K. N. Kudin, V. N. Staroverov, R. Kobayashi, J. Normand, K. Raghavachari, A. P. Rendell, J. C. Burant, S. S. Iyengar, J. Tomasi, M. Cossi, N. Rega, N. J. Millam, M. Klene, J. E. Knox, J. B. Cross, V. Bakken, C. Adamo, J. Jaramillo, R. Gomperts, R. E. Stratmann, O. Yazyev, A. J. Austin, R. Cammi, C. Pomelli, J. W. Ochterski, R. L. Martin, K. Morokuma, V. G. Zakrzewski, G. A. Voth, P. Salvador, J. J. Dannenberg, S. Dapprich, A. D. Daniels, Ö. Farkas, J. B. Foresman, J. V. Ortiz, J. Cioslowski, D. J. Fox, Gaussian, Inc., Wallingford, CT, USA, **2009**.
- [22] J. P. Perdew, K. Burke, M. Ernzerhof, *Phys. Rev. Lett.* **1996**, 77, 3865–3868.
- [23] A. Schäfer, H. Horn, R. Ahlrichs, *J. Chem. Phys.* **1992**, 97, 2571–2577.
- [24] C. Adamo, V. Barone, *J. Chem. Phys.* **1999**, 110, 6158–6170.
- [25] S. Grimme, S. Ehrlich, L. Goerigk, *J. Comput. Chem.* **2011**, 32, 1456–1465.
- [26] A. Schäfer, C. Huber, R. Ahlrichs, *J. Chem. Phys.* **1994**, 100, 5829–5835.

- [27] a) G. Te Velde, F. M. Bickelhaupt, E. J. Baerends, C. Fonseca Guerra, S. J. van Gisbergen, J. G. Snijders, T. Ziegler, *J. Comput. Chem.* **2001**, *22*, 931–967; b) G. Schreckenbach, T. Ziegler, *Int. J. Quantum Chem.* **1997**, *61*, 899–918; c) G. Schreckenbach, T. Ziegler, *Int. J. Quantum Chem.* **1996**, *60*, 753–766; d) G. Schreckenbach, T. Ziegler, *J. Phys. Chem.* **1995**, *99*, 606–611; e) J. Autschbach, S. Patchkovskii, B. Pritchard, *J. Chem. Theory Comput.* **2011**, *7*, 2175–2188; f) J. Autschbach, E. Zurek, *J. Phys. Chem. A* **2003**, *107*, 4967–4972.
- [28] a) E. van Lenthe, A. Ehlers, E.-J. Baerends, *J. chem. phys.* **1999**, *110*, 8943–8953; b) E. van Lenthe, E.-J. Baerends, J. G. Snijders, *J. chem. phys.* **1994**, *101*, 9783–9792; c) E. van Lenthe, E.-J. Baerends, J. G. Snijders, *J. chem. phys.* **1993**, *99*, 4597–4610.

---

Received: November 4, 2015

Published online on January 27, 2016